Springer

KSME

Journal of Mechanical Science and Technology 27 (8) (2013) 2331~2340
www.springerlink.com/content/1738-494x
DOI 10.1007/s12206-013-0616-7

Comparative study on the high-temperature tensile and creep properties of Alloy 617 base and weld metals †

Woo-Gon Kim[1,*], Jae-Young Park[2], I. M. W. Ekaputra[2], Sung-Deok Hong[1], Seon-Jin Kim[2] and Yong-Wan Kim[1]

[1]*Korea Atomic Energy Research Institute, 989-111 Daeduk-daero, Yuseong-gu, Daejeon 305-353, Korea*
[2]*Dept. of Mechanical Design Engineering, Pukyong National University, Busan, 608-739, Korea*

(Manuscript Received February 12, 2013; Revised March 22, 2013; Accepted April 1, 2013)

Abstract

This paper presents a comparative investigation on the high-temperature tensile and creep properties of Alloy 617 base metal (BM) and weld metal (WM) fabricated by a gas tungsten arc weld process. The WM had higher yield strength and lower ultimate tensile strength than the BM does; however, its elongation was significantly lower than that of the BM. The creep curve of the BM and WM was somewhat different from that of typical heat-resistance steel, and did not show a textbook creep. The WM exhibited a longer creep rupture life, lower creep rate, and lower rupture ductility than the BM. However, as the creep rupture time reached approximately 36,800 h, the creep life of the WM was expected to be almost similar to that of the BM; and after 36,800 h, its creep life was expected to be worse than the BM. Loner creep tests is needed to investigate the long-term creep life of the WM. The creep failure mode of the BM and WM was obviously an intergranular cracking of the cavity formation and growth mechanisms, although it was more evident in the WM. The BM had a more ductile fracture surface than the WM.

Keywords: Alloy 617; Tensile; Creep; Weld metal; GTAW

1. Introduction

The very high temperature reactor (VHTR) is one of the most promising Generation-IV reactor types for the economic production of electricity and hydrogen. Its major components are the reactor internals, reactor pressure vessel, piping, hot gas ducts, and intermediate heat exchangers (IHX), as shown in Fig. 1 [1-4]. The IHX is a key component, and Alloy 617 is a prime candidate material compared with other potential superalloys due to its superior creep resistance above 800°C [5-7].

At present, the Korea Atomic Energy Research Institute is developing a nuclear hydrogen development and demonstration plan with a capacity of 200 MW_{th} with thermal and core outlet temperature of 950°C. The plan has been carried out on a government-funded project called "development of key technologies for nuclear hydrogen" since 2006 [8-10]. Because the components are designed for a life span of 40~60 years operation at 950°C and 3~8 MPa in helium impurities, one of the most important properties of the components is the creep behavior, especially for the welded structures.

Generally, because the weld metal (WM) may have original some defects, the creep strength can be worse than that of the base metal (BM). Thus, in the design rules of high-temperature components, the allowable stresses in the welds are restricted to the lower value of the following: (i) the allowable stress in the BM is based on 67% of the stress to rupture, 80% of the stress to cause onset of a tertiary strain, and 100% of the stress to cause a 1% total strain, and (ii) the product of $0.8\ \sigma_{min} \times R$, where σ_{min} is the expected minimum stress of the BM and R is the appropriate ratio of the creep rupture strength of the WM compared with that of the BM [11, 12]. The allowable deformation in the welds is also restricted to half of the deformation permitted for the BM, because the ductility of the welds at elevated temperatures is generally low. For the design, the data of the tensile and creep properties of Alloy 617 WM should be sufficiently provided, and a design code for Alloy 617 WM should be developed. However, the data for the WM have been very rare and limited until now, although the data of the BM are available in a draft Alloy 617 code case, which was suspended at the end of the 1980s because of a lack of support and interest [1].

This study comparatively investigated the high-temperature tensile and creep properties of Alloy 617 BM and WM, which were fabricated by a gas tungsten arc welding (GTAW) procedure. The BM and WM properties were obtained and com-

*Corresponding author. Tel.: +82 42 868 2493, Fax.: +82 42 68 8549
E-mail address: wgkim@kaeri.re.kr
† Recommended by Editor Jai Hak Park

Table 1. Chemical composition of Alloy 617 plate (wt. %).

		C	Ni	Fe	Si	Mn	Co	Cr	Ti	P	S	Mo	Al	B	Cu
ASTM spec.	Min	0.05	Bal.	-	-	-	10.0	20.0	-	-	-	8.00	0.80	-	-
	Max	0.15	Bal.	3.00	0.50	0.50	15.0	24.0	0.60	0.015	0.015	10.0	1.50	0.006	0.50
Haynes 617		0.08	53.11	0.949	0.084	0.029	12.3	22.2	0.41	0.003	< 0.002	9.5	1.06	< 0.002	0.0268

Table 2. Chemical composition of filler metal (wt. %).

	C	Ni	Fe	Si	Mn	Co	Cr	Ti	P	S	Mo	Al	Cu
AWS spec.	0.05	Rem	MAX	MAX	MAX	10.0	20.0	MAX	MAX	MAX	8.00	0.80	MAX
	0.15	Rem	3.0	1.0	1.0	15.0	24.0	0.60	0.03	0.015	10.0	1.50	0.50
KW-T617 filler metal	0.07	Bal	0.33	0.3	0.3	11.29	22.5	0.42	<0.003	0.001	8.8	1.1	< 0.01

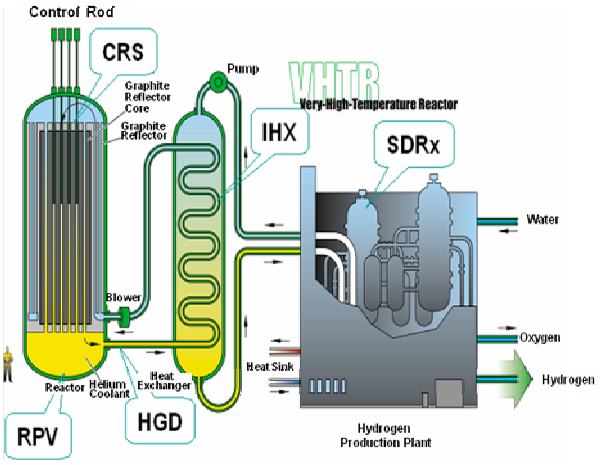

Fig. 1. Main components of the VHTR system for nuclear hydrogen production.

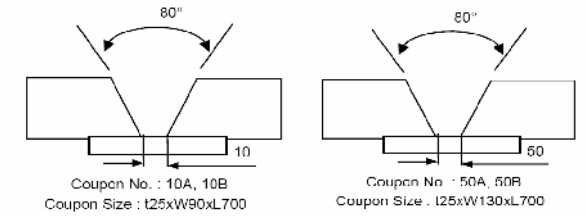

(a) 10 mm root gap (b) 50 mm root gap

Fig. 2. Single V-groove dimensions for fabricating the Alloy 617 weldments.

pared, and the fracture morphologies from the fracture specimens were also examined.

2. Experimental procedures

2.1 Welding method

Commercial-grade nickel-based superalloy, Alloy 617 (Haynes 617) was used in this study, which was a hot-rolled plate with a thickness of 25 mm. The chemical composition is given in Table 1, and the amount of each element was well within the ASTM specifications. The shape of the weld joint (WJ) has a single V-groove with an angle of 80°.

A filler metal was used for KW-T617 (brand name), manufactured by KISWEL Company. It was prepared according to the American Welding Society (AWS) specifications, AWS A 5.14-05 ERNiCrCoMo-1 (UNS N06617), and its diameter was 2.4 mm. The chemical composition is given in Table 2. The amount of each element was well within the AWS specifications. To shield the welding pool from the atmosphere during welding, a 99.99% pure argon gas from 10 L/min to 15 L/min was supplied.

Two types of root gaps of 10 and 50 mm were fabricated. The 10 mm root gap specimens were prepared to evaluate the WJ, and the 50 mm root gap specimens were prepared to evaluate the WM. Here, they are designed as 10A and 10B for the 10 mm root gap and 50A and 50B for the 50 mm root gap, as shown in Fig. 2. A backing gas to prevent oxidation to the back side of the WM was not supplied. The GTAW conditions are given as follows:

- Polarity: DC straight polarity.
- Current range: from 180 A to 200 A.
- Voltage range: from 14 V to16 V.
- Welding speed: from 18 cm/min to 22 cm/min.
- Pre-heating temperature: minimum of 18°C.
- Temperature between passes: under 177°C.

In the GTAW process, 14 welding layers and 41 passes were applied for the 10A and 10B specimens, and 15 layers and 133 passes were applied for the 50A and 50B specimens. To prevent a bending deformation of the weldments, some passes at the back side were added for each specimen, as shown in Figs. 3(a) and 3(b). Post heat-treatment was not conducted because the Ni-based superalloy was not normally applied. After welding, the soundness of the weldments was investigated by ultrasonic, tensile, and bending tests.

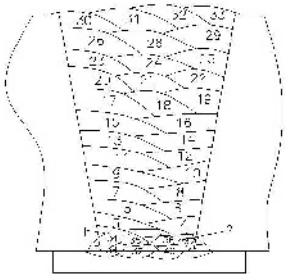

(a) 10A and 10B weldments (10 mm root gap)

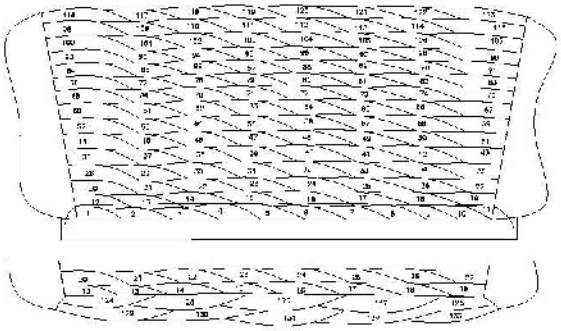

(b) 50A/50B wledments (50 mm root gap)

Fig. 3. Profiles of the welding layers and pass number for 10A/10B and 50A/50B weldments.

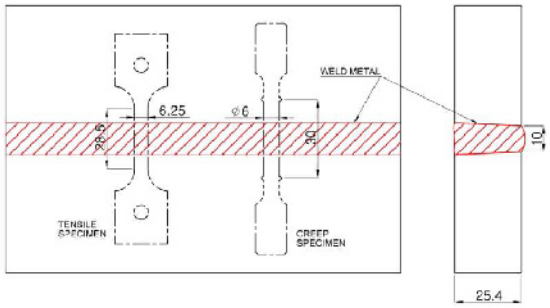

(a) WJ

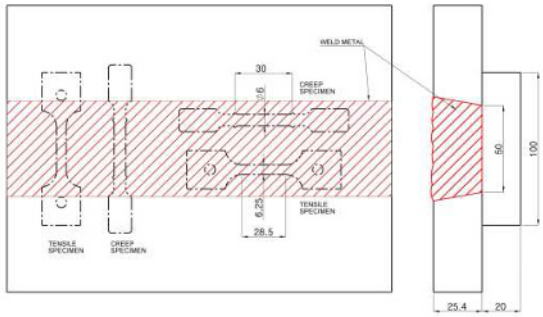

(b) WM

Fig. 4. Cutting method of the tensile and creep test specimens for the Alloy 617 weldments.

Fig. 5. OM structure of the Alloy 617 weldments.

2.2 Test method

Figs. 4(a) and 4(b) show the cutting methods used in the WJ and in the WM to prepare the tensile and creep test specimens. In the WJ specimens, the WM and WJ regions were cut within the gage length for inclusion. These specimens were prepared to evaluate the joint strength in the WJ region. In the WM specimens, the tensile and creep specimens were taken from fully welded metal. The specimens were machined into the transverse direction (TD) and longitudinal direction (LD) against the welding direction, and the tensile properties in the two directions were compared.

The tensile test specimens were machined into a rectangular cross section with a gage length of 28.5 mm, width of 6.25 mm, and thickness of 1.5 mm. The strain rate in the tensile tests was conducted with a slow strain rate of 5.85×10^{-4} 1/s at temperature ranges from room temperature to 950°C. Further, the creep test specimens were machined into a cylindrical form with a gage length of 30 mm and diameter of 6 mm.

A series of creep tests was performed under different stress levels of 35, 30, 25, 22, 20, and 18 MPa for the BM and 35, 30, 24, and 20 MPa for the WM at an identical temperature of 950°C. The pull rod and jig used for the creep tests were manufactured using Ni-based superalloy materials to endure sufficiently the oxidation and thermal degradation during the creep tests. Creep strain data with elapsed times were taken automatically by a PC through a high-precision extensometer. The steady-state creep rate was measured from the experimental creep curves.

A photograph of the Alloy 617 weld block taken with a 10 mm root gap after welding is shown in Fig. 5. The profiles of the multi layers can be observed. A Vickers micro-hardness survey was performed across the Alloy 617 weldment, as indicated by the white straight line in the photo.

After testing, to observe the optical microscope (OM) and scanning electron microscopy (SEM) micrographs, an electro etching was conducted for 12~15 s using two voltages in a mixed solution of H_2O (90%) + HCl (10%).

3. Results and discussion

3.1 Tensile properties

Figs. 6(a)-6(c) show the optical microstructure of the BM, WM, and heat affected zone (HAZ), respectively. In the photograph of the BM structure, the grain boundary (GB) is uniform and stable; however, in the WM structure, the GB is meanderingly non-uniform as a cell-type-dendrite solidification structure. This weld structure appeared to have been formed from the solidification when the welding material is

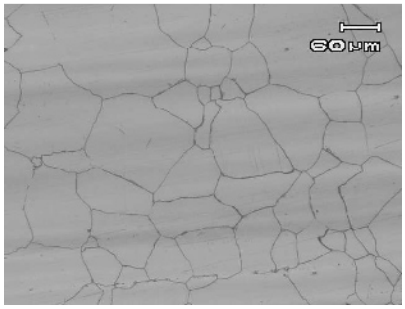

(a) BM

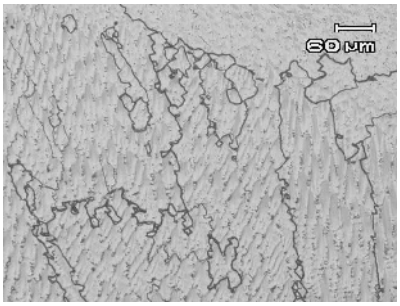

(b) WM

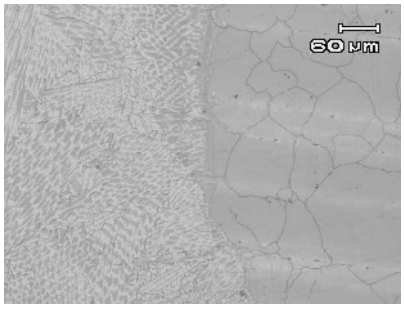

(c) HAZ

Fig. 6. Optical microstructure showing the solidified grain boundaries of the Alloy 617 weldment.

solidified between the solid and liquid interfaces. Then, in the HAZ structure, a fusion line between the BM and WM is observed. The WM solidification appeared to have been started from this fusion line, and its crystallization was an epitaxial growth that grew directly along the same directions as that in the coarse GBs in the HAZs. The HAZ is believed to be different in terms of the mechanical properties compared with the BM, because of the number of thermal cycles in the multi-layer welding process used in this study.

Fig. 7 shows the results of the micro-hardness measurements of the Alloy 617 weldment, with the dashed lines delineating the approximate location of the HAZs on each side of the WM. The BM hardness was approximately from 280 to 290, rising to approximately 350 in the HAZ; it was approximately from 320 to 340 in the WM. The WM had a higher value (approximately from 40 to 50) than the BM. The hardness in the HAZ sharply changed in the transition region between the BM and WM. The HAZ width was very narrow at approximately from 3 mm to 5 mm, and the grains coarsened.

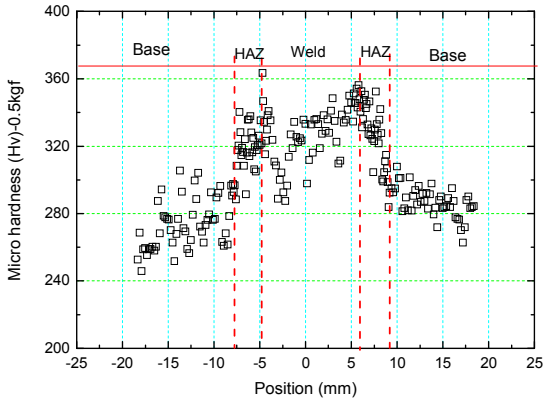

Fig. 7. Micro-hardness variation (Hv) across the WJ.

Fig. 8 shows the results of the high-temperature tensile property measurements. Figs. 8(a)-8(c) shows 0.2% yield stress (YS), ultimate tensile strength (UTS), and tensile failure elongation for the BM, WJ, and WM (LD and TD) of the Alloy 617 weldments, respectively. The YS value of the BM was lower than that of the WM; however, at above 800°C, the YS values of the BM, WJ, and WM were almost the same. A large difference in the stress values between the TD and LD of the WM appeared. Meanwhile, the UTS value of the BM was higher than those of the WM and WJ. At above 800°C, the UTS values of the BM, WJ, and WM were almost the same. In terms of the tensile elongation, the WM ductility dropped significantly compared with that of the BM. That of the WJ was the lowest.

Fig. 9 shows the typical SEM fracture surfaces of the BM and WM at room temperature (RT), 400, 600, 800, and 950°C. At RT, the WM surface exhibited clearly an equal-axial dendrite structure, which mainly solidified along the GBs. It was formed at the final cooling phase of the solidification of the WM. Some differences existed in the fractures between the BM and WM. The WM showed a significantly cleave failure surface, but the BM showed a more ductile fracture than the WM. In addition, at 950°C, dimples were significantly observed in the BM compared with the WM.

3.2 Creep rupture properties

To understand the creep behavior of BM and WM of Alloy 617, the creep properties such as the creep rupture time, creep strain rate (steady-state creep rate), rupture elongation, and reduction in area were investigated through a series of creep tests at an identical temperature of 950°C. Long-time rupture data that reached approximately 14,000 h (1.6 years) for the BM and 10,172 h (1.16 years) for the WM were experimentally obtained. After the creep testing, the fracture micrographs of each tested specimen were examined using OM and

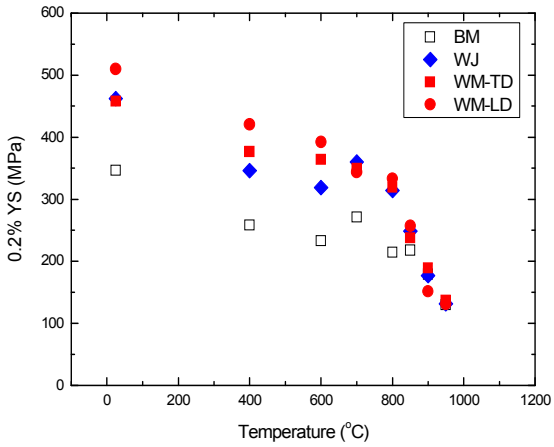

(a) 0.2% YS

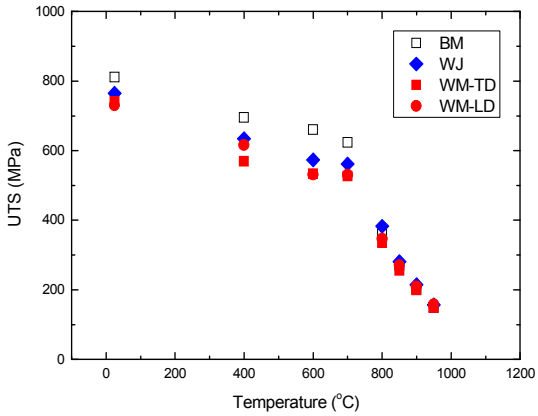

(b) UTS

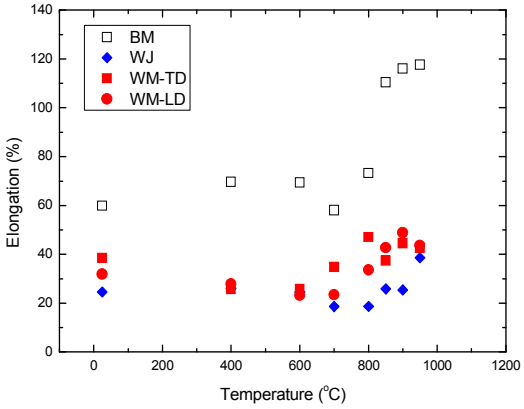

(c) Elongation

Fig. 8. High-temperature tensile properties of the Alloy 617 weldments.

SEM. In this study, the creep test results for the BM and WM were comparatively presented in detail.

Figs. 10 and 11 show the comparisons of the creep curves of the BM and WM of Alloy 617 tested at 950°C. Fig. 10 shows that of the 30 MPa and Fig. 11 shows that of the 20 MPa. The shape of the creep curves for the BM and WM was not different in the primary, secondary, and tertiary creep re-

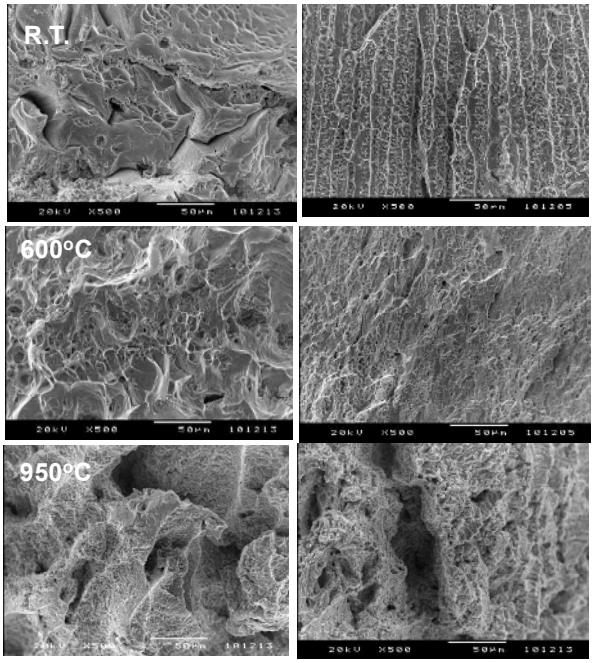

(a) BM (b) WM

Fig. 9. SEM micrographs of the fracture surfaces at tensile test temperatures for the BM and WM.

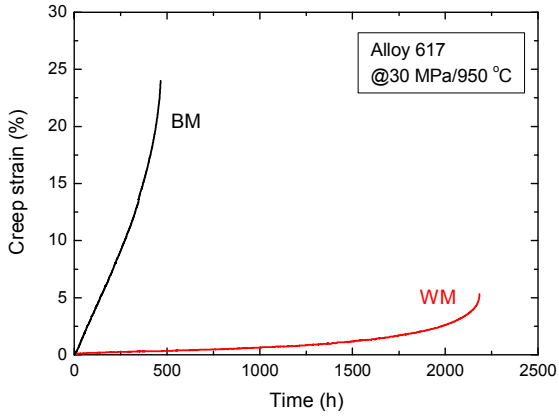

Fig. 10. Comparison of the creep curves of the BM and WM of Alloy 617 tested under 30 MPa at 950°C.

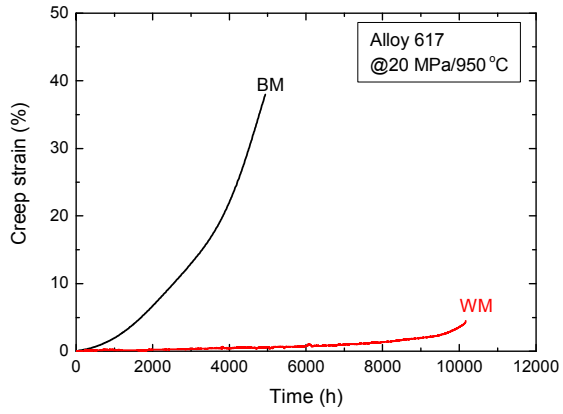

Fig. 11. Comparison of the creep curves of the BM and WM of Alloy 617 tested under 20 MPa at 950°C.

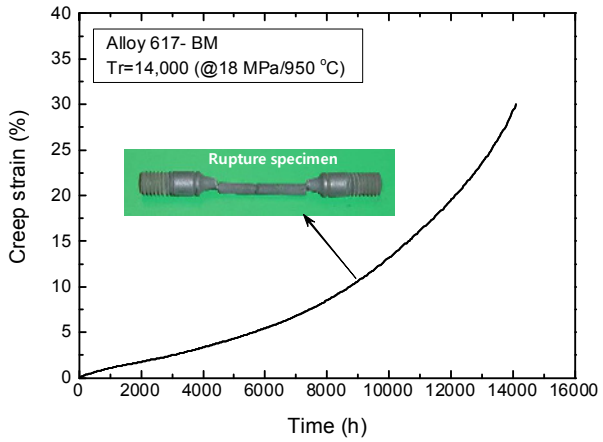

Fig. 12. Typical creep curve of the BM of Alloy 617 tested under 18 MPa at 950°C [t_r = 14,000 h (1.6 years)].

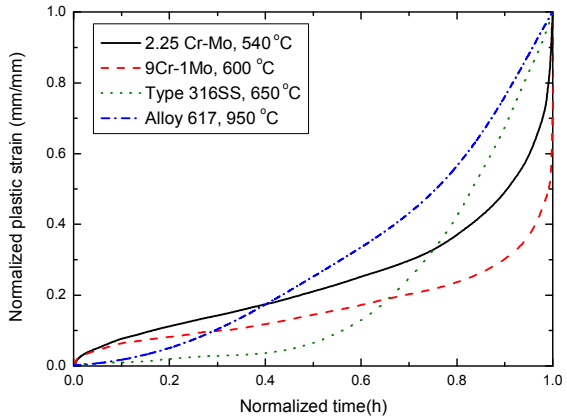

Fig. 13. Comparison of the normalized creep curves for typical heat resistant steels.

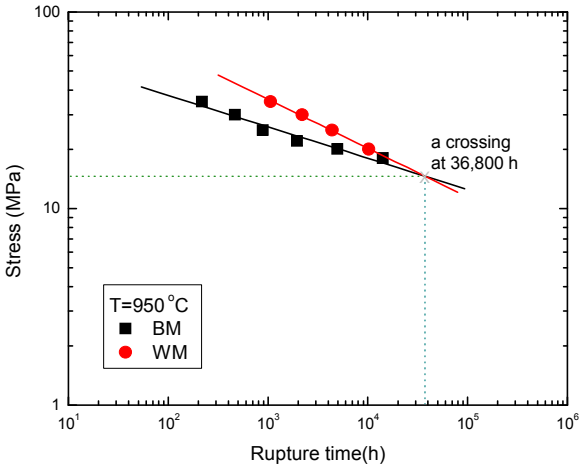

Fig. 14. Plot of log stress versus log rupture time obtained for the BM and WM at 950°C.

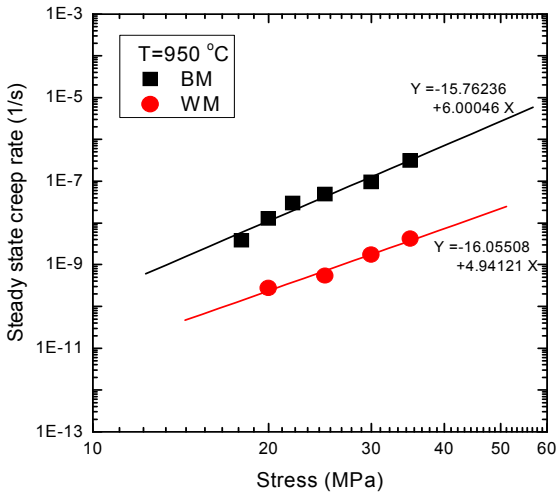

Fig. 15. Plot of the steady-state creep rate versus applied stress for the BM and WM tested at 950°C.

gimes. Compared with the BM, the WM had a longer creep rupture time, but had a lower creep rupture elongation. Creep deformation appeared to develop dominantly from the cavity formation and growth in the creep process, as shown in the ruptured specimen in Fig. 12. The cavities were uniformly distributed over the total gage section of the specimen, and they occurred because of the accumulated damage induced during the creep process under the high-temperature and stress conditions. Cracks were initiated by linking and incorporation with the micro voids, and then developed along the voids. Finally failure occurred because of the interconnections of the voids rather than the necking failure in the tertiary creep region. Owing to the results, it is identified that the Alloy 617 WM has a small reduction in its area.

The creep curve of Alloy 617 appears somewhat different from that of typical heat-resistant steels, such as 2.25Cr-1Mo steel, 9Cr-1Mo steel, and austenitic stainless steel (type 316LN), as shown in Fig. 13. The creep curves of the low and high-Cr ferritic steels plot are distinct primary, secondary, and tertiary creep stages (called "textbook creep curve"). However, Alloy 617 does not exhibit a textbook creep curve, as shown in Figs. 12 and 13, but a predominantly accelerated creep rate from the start of the tertiary creep stage in short time ranges.

Fig. 14 shows the plot of the log stress versus log rupture time obtained for the BM and WM at 950°C. The WM had a higher creep strength (or longer creep rupture life) than the BM. However, as the creep life increased, the two fitting lines between the BM and WM crossed at 36,800 h. After 36,800 h, we estimate that the creep life of the WM is shorter than that of the BM. We thus believe that longer creep tests will be needed to investigate the long-term creep life of the WM.

Fig. 15 shows the comparative plot of the steady-state creep rate as a function of the applied stress for the BM and WM tested at 950°C. The steady-state creep rate $\dot{\varepsilon}_s$ is described by the Norton's power-law function of applied stress as

$$\dot{\varepsilon}_s = A\sigma^n \quad (1)$$

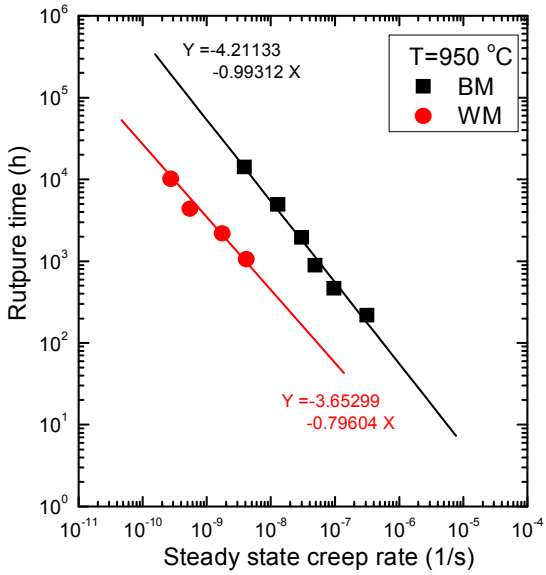

Fig. 16. Plot of the M-G relationship for the BM and WM at 950°C.

where σ is the applied stress, and *n* is the stress exponent. The value of *A* and *n* can be obtained from Fig. 15. A small different slope for the two lines was determined from the data sets obtained at different applied stresses for the BM and WM. The *A* and *n* values were determined as 4.82×10^{-20} (MPa^{-n} h^{-1}) and 6.0 for the BM, respectively, and 2.77×10^{-20} (MPa^{-n} h^{-1}) and 4.9 for the WM, respectively. However, these values indicate that the stress exponent for the creep was almost the same, and the same creep mechanism is regarded as operating in both the BM and WM tested at 950°C in this study. Further, the value of n = 4.9 to 6.0 obtained for the BM and WM was reasonable because it was similar to the value of n = 3 to 6 reported for single phase materials [13]. Quantitatively, the WM was 1.75 times lower in the creep strain rate than the BM, although the rupture data were taken for only four tests in this study. It is believed that the longer rupture life of the WM was due to the lower creep rate.

Fig. 16 shows a plot of a Monkman-Grant (M-G) relationship of the log-rupture time versus log-creep strain rate for the BM and WM of Alloy 617. The M-G relationship can be expressed by [14, 15]

$$\log t_r + m \log \dot{\varepsilon}_s = K \tag{2}$$

where t_r is the creep rupture life, and *m* and *K* are the material constants. Eq. (2) shows that the creep rupture life is in inverse proportion to the creep strain rate. If the constants for the materials are known, we can predict the other from one. The M-G function can be reasonably used when the relationship follows well the fact that cavity formation and growth are on the basis of the creep process [14].

As described above, because Alloy 617 revealed creep deformation of the cavity formation and growth in the creep process, it is regarded to be fairly adaptable to the BM and

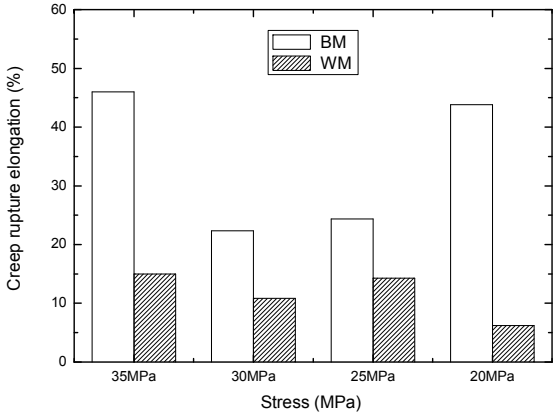

(a) Creep rupture elongation (%)

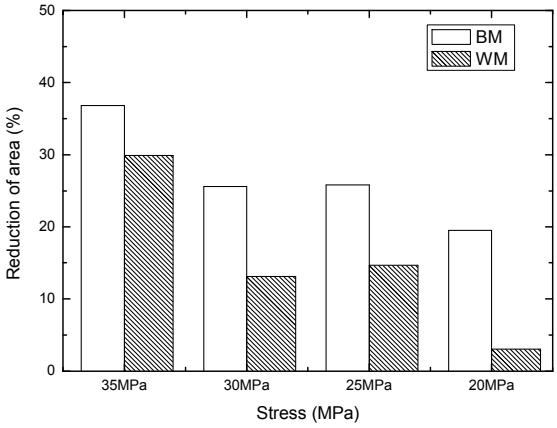

(b) Reduction of area (%)

Fig. 17. Comparison of creep rupture elongation and reduction in area for the BM and WM tested at 950°C.

WM of Alloy 617. A small different slope for the two lines was determined for the BM and WM. The *m* and *K* values were 0.99 and 4.21 for the BM, and 0.80 and 3.65 for the WM. The WM line was shifted to the left side with one order of the creep strain rate.

Fig. 17 shows a comparison of the creep rupture elongation and reduction in the area for the BM and WM tested at 950°C. The WM of the Alloy 617 had a significant reduction in the rupture elongation and reduction in the area compared with the BM. This result is similar to the results in the heat-resistant steel in which the ductility of welds at elevated temperature was generally low. This result should be carefully treated because a large reduction in the rupture ductility of the WM of Alloy 617 may cause a brittle fracture.

Accordingly, during the current test period at the present test conditions, the WM of Alloy 617 revealed a higher creep life (or strength) owing to the lower creep strain rate. However, the creep behavior for a longer creep life of over 10^4 h has not been found by other researchers until now. Further the longer rupture data are insufficient, and they are not available. We thus emphasize that a number of the longer creep tests will be needed to investigate the long-term creep life of the WM.

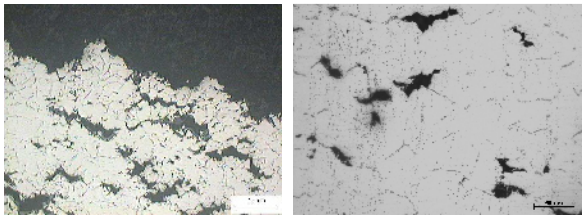

(a) Low magnification (b) High magnification

Fig. 18. Typical OM structures of the BM tested under 20 MPa at 950°C (t_r = 4,943 h).

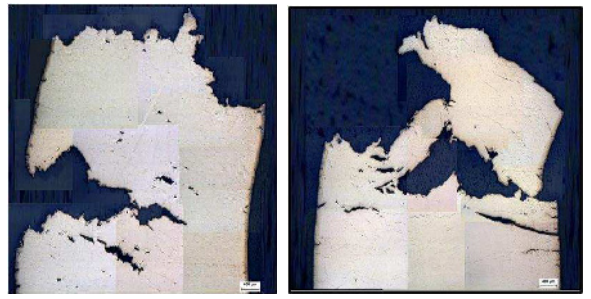

(a) 35 MPa (b) 30 MPa

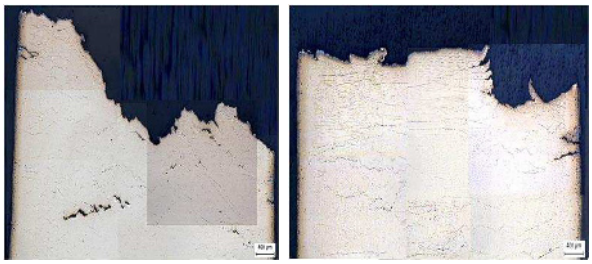

(c) 25 MPa (d) 20 MPa

Fig. 19. Crept specimens with applied stresses for the WM.

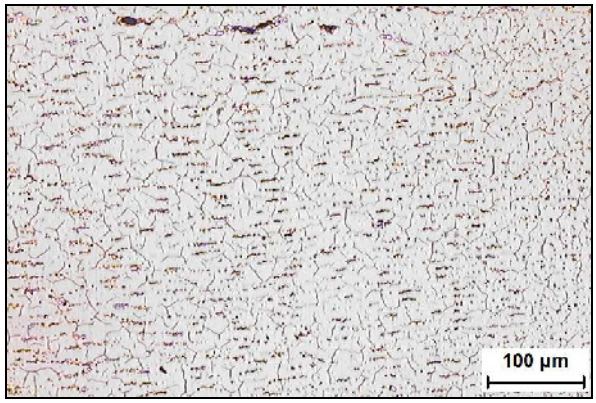

Fig. 20. Typical OM structure of the WM tested under 25 MPa at 950°C.

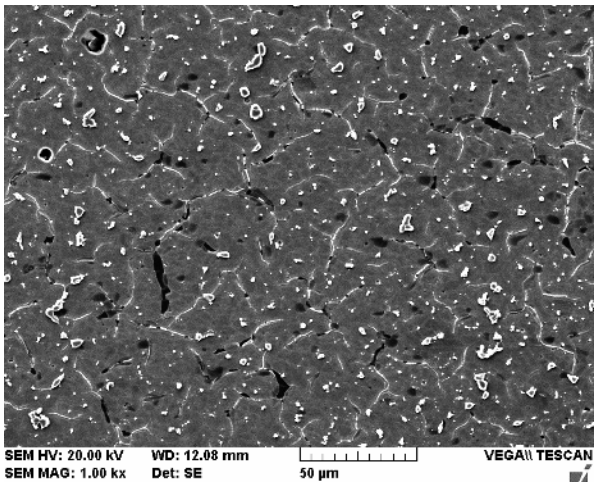

Fig. 21. SEM image showing the precipitates, cavities, and voids of the WM tested under 25 MPa at 950°C.

3.3 Fracture micrographs

Fig. 18 shows the OM structures of the BM crept under 20 MPa at 950°C. In the low (Fig. 18(a)) and high (Fig. 18(b)) magnifications, the cavities and cracks are formed along the grain boundary perpendicular to the applied stress and widely distributed in the overall gage section. A creep failure occurred from the interconnections of the cavities and cracks formed during the creep at the present test conditions. The failure was dominant in the intergranular fracture. In the WM, similar failure occurred along the cracks developed perpendicular to the applied stress, as shown in Fig. 19. Many minor cracks were widely distributed in the overall gage section. The failure obviously occurred because of the cracks formed by cavity formation and growth mechanism. At high stresses (Figs. 19(a) and (b)), the failures occurred irregularly on some large cracks. Otherwise, at low stresses (Figs. 19(c) and (d)), they smoothly occurred on one fracture plane, at a low stress of 20 MPa.

Fig. 20 shows a typical OM structure for the WM specimen crept at 25 MPa. In the matrix, many minor cavities and some creep cracks existed along the GBs. However, the image was not clear for the cracks and the precipitates formed in the matrix to be observed. To observe them more clearly, a SEM micrograph was taken.

Fig. 21 shows a typical SEM micrograph of the WM tested under 25 MPa at 950°C, which shows that the precipitates are formed along the GBs, and the cavities and voids are generated at the site of the GBs. We assumed that they played a role as nucleation site that caused cavities and voids during the creep process. We have identified that the precipitates were significantly distributed at a longer rupture time (a low-stress condition) compared with the short rupture time (a high stress condition). Generally, creep properties are closely related to the amount, shape, and size of the distribution of the precipitates.

Fig. 22 shows the SEM micrographs of the fracture surfaces for the BM and WM specimens tested at identical conditions of 20 MPa at 950°C. The low magnification is for the left - hand side, and the high magnification is for the right-hand side. The BM and WM showed combined fracture modes consisting of a dimple rupture and intergranular cracking. However,

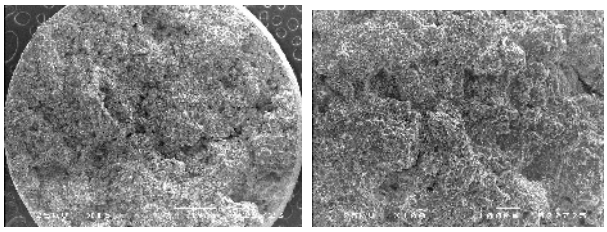

(a) BM (20 MPa at 950°C)

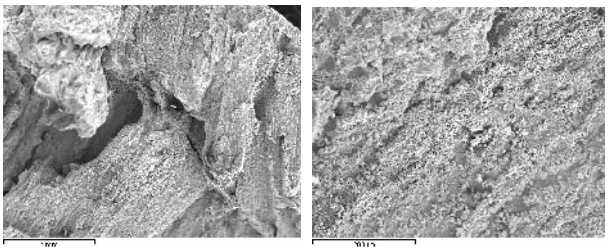

(b) WM (20 MPa at 950°C)

Fig. 22. SEM fracture surfaces for the BM and WM tested under 20 MPa at 950°C.

the intergranular cracking is more evident in the WM specimens, which is consistent with the observation of lower creep ductility in the WM than that in the BM. The WM specimen shows a solidification fracture surface formed for solidification of the welds. The BM specimen shows a more ductile fracture surface than the WM does. In addition, oxides of Cr_2O_3 formed in the creep tests are observed in the fracture surfaces, as shown in the high magnification photographs for the BM and WM. The amount of oxides increased with the increase in the rupture time.

4. Conclusions

The high-temperature tensile and creep properties of Alloy 617 BM and WM, fabricated by the GTAW process, have been investigated by a series of tensile and creep tests, and the properties of the BM and WM were compared. Their fracture morphologies were also examined from the fracture specimens. The following conclusions were drawn:

The WM of Alloy 617 had a higher YS value than the BM, but had a lower UTS value. The WM was significantly reduced in terms of the tensile elongation compared with the BM. The creep curves of the BM and WM appeared to be somewhat different from those of typical heat-resistant steel, and they did not show a textbook creep behavior. The WM showed a longer rupture life, lower creep strain rate, and lower rupture ductility than the BM. The longer rupture life was due to the lower creep strain rate in the WM. As the creep rupture time approached 36,800 h, we estimated that the creep life of the WM was the same as that of the BM; however, after 36,800 h, the WM was worse than the BM. We therefore believe that longer creep tests will be needed to investigate the long-term creep life of the WM. In the micrograph observations, the BM and WM revealed a similar behavior in forming the cracks and cavities along the GB perpendicular to the applied stress, and the cracks and cavities were widely distributed in the overall gage section. The creep failure mode of the BM and WM was obviously an intergranular cracking of the cavity formation and growth mechanisms. However, intergranular cracking was more evident in the WM, which showed a lower rupture ductility than the BM. In addition, the BM revealed a more ductile fracture surface than the WM.

Acknowledgment

This work was performed under the long-term Nuclear R & D Program sponsored by the Korean Ministry of Science and Technology.

References

[1] W. G. Kim, S. N. Yin, J. Y. Park, S. D. Hong and Y. W. Kim, An improved methodology for determining tensile design strengths of Alloy 617, *Journal of Mechanical Science and Technology*, 26 (2012) 379-387 .

[2] W. G. Kim, S. N. Yin, Y. W. Kim and J. H. Chang, Creep properties and creep life prediction of Alloy 617 for a very high temperature gas-cooled reactor, *Proc. of ASME PVP 2008 Conf.*, Chicago, USA, July (2008) Paper PVP 2008-61356.

[3] S. J. Dewson and X. Li, Selection criteria for the high temperature reactor intermediate heat exchanger, *Proc. of ICAPP 05*, Seoul, Korea, May (2005) Paper 5333.

[4] W. G. Kim, S. N. Yin, W. Y. Kim and J. H. Chang, Creep characterization of a Ni-based Hastelloy-X alloy by using theta projection method, *Engineering Fracture Mechanics*, 75 (2008) 4985-4995.

[5] W. G. Kim, S. N. Yin, G. G. Lee, Y. W. Kim and S. J. Kim, Creep oxidation behavior and creep strength prediction for Alloy 617*, Int. J. of Pressure Vessels and Piping,* 87 (2010) 289-295.

[6] J. M. Corum and J. J. Blass, *Rules for design of alloy 617 nuclear components to very high temperatures*, Attachment 2, Draft Code Case for Alloy 617, USA (1988).

[7] W. G. Kim, S. N. Yin, W. S. Ryu and J. H. Chang, Analysis of the creep rupture data of Alloy 617 for a high temperature gas cooled reactor, *The 8th Int. Conf. on Creep and Fatigue at Elevated Temperatures*, Texas, USA, July (2007) Paper PVP 2007-26834.

[8] J. H. Chang, Y. W. Kim, K. Y. Lee, Y. W. Lee, W. J. Lee, J. M. Noh, M. W. Kim, H. S. Lim, Y. J. Shin, K. K. Bae and K. D. Jung, A study of a nuclear hydrogen production demonstration plant, *Nuclear Engineering and Technology*, 39 (2) (2007) 111-122.

[9] H. Y. Lee, Y. W. Kim and K. N. Song, Preliminary application of the draft code case for alloy 617 for a high temperature component, *J. of Mechanical Science and Technology,* 22 (2008) 856-863.

[10] J. Y. Park, D. W. Kim, D. J. Kim, E. S. Kim, H. P. Kim, S. H. Kim, W. J. Kim, W. G. Kim, W. S. Ryu and Y. D. Kim,

Development of materials for a high temperature gas cooled reactor in Korea, *The 4th International Topical Meeting on High Temperature Reactor Technology-HTR 2008*, Washington, USA (2008) Paper HTR 2008-58149.

[11] W. G. Kim and W. S. Ryu, Creep rupture properties of type 316LN stainless steel welded by the SAW process, *Solid State Phenomena,* 119 (2007) 91-97.

[12] M. D. Mathew, G. Sasikala, S. L. Mannan and P. Rodriguez, A comparative study of the creep rupture properties of type 316 stainless steel base and weld metals, *J. of engineering Materials and Technology*, 115 (1993) 163-170.

[13] H. E. Evans, *Mechanism of creep fracture*, Elsvier Applied Science Publishers LTD, London and New York, UK and USA (1984).

[14] W. G. Kim, S. H. Kim and W. S. Ryu, Evaluation of Monkman-Grant parameters for type 316LN and modified 9Cr-1Mo stainless steels, *J. of Mechanical Science and Technology,* 16 (11) (2002) 1420-1427.

[15] G. E. Deter and D. Bacon, *Mechanical metallurgy*, Third Ed. McGraw-Hill Book Company, London, UK (1988).

Woo-Gon Kim obtained the Ph.D. at the Department of Mechanical Engineering, Chungbuk National University in 1998. He is currently a Principal Researcher with Korea Atomic Energy Research Institute. His specialty is mechanical assessment, analysis, modeling, and database establishment of high-tempera- ture nuclear materials for Gen-IV reactor systems and time-dependent creep and crack growth behaviors at elevated temperature.